Ultrasensitive and Selective Recognition of Peptide Hormone Using Close-Packed Arrays of hPTHR-Conjugated Polymer Nanoparticles

Oh Seok Kwon,[†] Sae Ryun Ahn,[‡] Seon Joo Park,[†] Hyun Seok Song,[‡] Sang Hun Lee,[‡] Jun Seop Lee,[†] Jin-Yong Hong,[†] James S. Lee,[†] Sun Ah You,[†] Hyeonseok Yoon,[§] Tai Hyun Park,[‡,*] and Jyongsik Jang[†,*]

[†]World Class University Program of Chemical Convergence for Energy & Environment, School of Chemical and Biological Engineering, Seoul National University, Seoul 151-742, Korea, [‡]School of Chemical and Biological Engineering, Bio-MAX Institute, Seoul National University, Seoul 151-744, Korea, and [§]Department of Polymer and Fiber System Engineering, Chonnam National University, Gwangju 500-757, Korea

ABSTRACT Recognition of diverse hormones in the human body is a highly significant challenge because numerous diseases can be affected by hormonal imbalances. However, the methodologies reported to date for detecting hormones have exhibited limited performance. Therefore, development of innovative methods is still a major concern in hormone-sensing applications. In this study, we report an immobilization-based approach to facilitate formation of close-packed arrays of carboxylated polypyrrole nanoparticles (CPPyNPs) and their integration with human parathyroid hormone receptor (hPTHR), which is a B-class family of G-protein-coupled receptors (GPCRs). Our devices enabled use of an electrically controllable liquid-ion-gated field-effect transistor by using the surrounding phosphate-buffered saline solution (pH 7.4) as electrolyte solution. Field-induced signals from the peptide hormone sensors were observed and provided highly sensitive and selective recognition of target molecules at unprecedentedly low concentrations (*ca.* 48 fM). This hormone sensor also showed long-term stability and excellent selectivity in fetal bovine serum. Importantly, the hormone receptor attached on the surface of CPPyNPs enabled GPCR functional studies; synergistic effects corresponding to increased hPTH peptide length were monitored. These results demonstrate that close-packed CPPyNP arrays are a promising approach for high-performance biosensing devices.

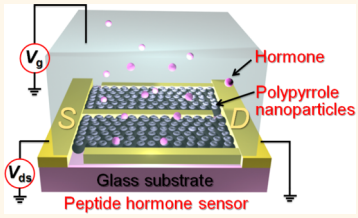

KEYWORDS: hormone receptor · field-effect transistor · nanoparticles · hormone sensor · conducting polymer

Very low concentrations of hormones are able to control and regulate the activity of many cells or organs in the human body, and hormone imbalance leads to serious diseases such as osteoporosis, adenoma, cardiovascular, hyperplasia, and cancer.[1−6] Therefore, over the past decade, significant efforts have been made to develop novel techniques for recognizing hormones.[7] Several innovative methods have been established to meet this need, including immunometric assays such as enzyme immunoassays (EIA) and enzyme-linked immunosorbent assays (ELISA),[8] fluorescence optochemical sensors,[9] multianalyte immunosensors,[10] electrochemical enzyme immunoassays,[11] and sensors based on surface plasmon resonance.[12,13] Although these techniques provide the possibility of hormone detection, the development of an easy, rapid, and accurate detector with high sensitivity remains a challenge.

Recent nanoparticle (NP)-based devices are significantly advancing fields such as clinical analysis, security control, and energy/environmental convergence.[14] Electrical and electrochemical technologies using NPs represent interesting alternatives for the development of efficient, fast, and low-cost devices to analyze real samples. The field-effect transistor (FET)-based biosensor, in particular, provides efficient stability and miniaturization.[15,16] To fabricate high-performance FET biosensors, NPs are synthesized with active channels that have the desired optical, photothermal, and electrical properties.[17−23] From a materials perspective, metallic and ceramic NPs have been extensively developed; their structures and sizes can be precisely controlled.[24−35] However, progress in NP fabrication from conducting polymers (CPs) has been relatively slow because of inherent structural instabilities at the nanoscale.[36−40] Moreover, positioning the NPs in an electrode gap is key to obtaining the electrical properties required for FET devices based on direct measurements of changes in conductivity. Therefore, the major concerns

* Address correspondence to jsjang@plaza.snu.ac.kr, thpark@snu.ac.kr.

Received for review April 4, 2012 and accepted May 31, 2012.

Published online May 31, 2012
10.1021/nn301482x

when using CP NPs in FETs are the fabrication of highly uniform, well-ordered, and size-controlled NPs and their continuous arrays on the electrode substrate.

The biological activity of hPTH, a peptide hormone, is vital for maintaining calcium homeostasis in mammals and can be a factor in potentially fatal diseases such as adenoma, hyperplasia, osteoporosis, and cancer.[41] Human parathyroid hormone receptor (hPTHR), which belongs to the B-class family of G-protein-coupled receptors (GPCRs), is involved in the regulation of calcium concentration in the blood.[1−7,42−46] GPCRs mediate various physiological processes, including cell signal transduction, sensory signaling, neuronal transmission, and hormonal signaling.[47−49] Despite the importance of GPCR-functional studies for the improvement of new pharmaceuticals, the invention of suitable assay tools has been limited by time-consuming and complex *in vitro* treatments.[42] Therefore, the development of facile, rapid and reproducible techniques remains a challenge.

Herein, we describe an immobilization-based process for carboxylated polypyrrole nanoparticles (CPPyNPs) and their integration, together with hPTHR, into an electronically controllable FET platform. Field-induced sensitivity from the peptide hormone sensor was observed, which enabled highly sensitive and selective recognition of target molecules at unprecedentedly low concentrations (*ca.* 48 fM). Moreover, the FET-type sensors exhibited long-term stability, excellent selectivity, and synergistic effects depending on the peptide length of hPTH. Importantly, this research can provide an advanced technical method for basic research on GPCR function and open up opportunities for various applications in drug discovery/biomedical diagnostics. To our knowledge, this is the first example of a liquid-ion-gated FET-type peptide hormone sensor based on close-packed arrays of hPTHR-conjugated CP NPs.

RESULTS AND DISCUSSION

Fabrication of Close-Packed Arrays of hPTHR-Conjugated CPPyNPs. Previously, we demonstrated a liquid-ion-gated biosensor based on various biomolecule/CP nanotube hybrids.[47−49] The main factors for the fabrication of high-performance FET-type biosensors are the stability of the nanoscale devices in the sensing environment (usually liquid-ion solution) and the covalent linkage between transducers and bioreceptors through surface functionalization.[39]

A high surface-to-volume ratio in nanoscale FET sensors is also crucial for sufficient binding capacity in the receptor/analyte interactions.[28,50−52] For this reason, the highly monodisperse, uniform, and size-tunable CPPyNPs were fabricated by chemical copolymerization of pyrrole with pyrrole-3-carboxylic acid using a dispersion method. Importantly, the introduction of carboxyl (−COOH) groups can not only provide compact CPPyNPs arrays on the substrate but also enable the attachment of receptors on the CPPyNP surface. The CPPyNPs were uniformly shaped and roughly 20, 60, and 100 nm in diameter with conductivities of 8×10^{0}, 7×10^{-1}, and 2×10^{-1} S cm^{-1}, respectively, as calculated from four-probe conductivity measurements. The Brunauer−Emmett−Teller (BET) surface areas of the 20, 60, and 100 nm particles were approximately 144, 104, and 68 m^2 g^{-1}, respectively.[53]

Scheme 1 illustrates the close-packed CPPyNP arrays adhered between the electrode gaps. An interdigitated microelectrode array (IMA) with a pair of gold electrode bands was prepared by standard lithographic processes on a glass substrate (Supporting Information, Figure S1). The IMA substrate was engineered using 3-aminopropyltrimethoxysilane (APS) to construct the specific functionalized surface. The CPPyNPs were compactly bound to the IMA substrate through covalent linkages between amino groups on the substrate surface and the carboxylic groups of the CPPyNPs. hPTHR, which contains terminal amine groups, was then covalently anchored to the CPPyNP surface by a similar condensation reaction. This immobilization approach offers critical advantages relative to conventional noncovalent attachment, including the formation of efficient electrical pathways in the surrounding liquid solution and the simplicity of the specific integration between the transducer and bioreceptors.

Characterization of Close-Packed Arrays of hPTHR-Conjugated CPPyNPs. High-level expression of hPTHR from *Escherichia coli* was demonstrated by Western blot analysis using anti-GST antibody (Figure S2). Milligram quantities of hPTHR were found mainly in the insoluble fraction, and the expression pattern was similar to other GPCRs described in our previous report.[54−56] The IMA electrode was functionalized with APS to modify the surface of the substrate. The reactions are as follows:

$$\text{hydrolysis}: H_2N(CH_2)_3Si(OCH_3)_3 + 3H_2O \rightarrow H_2N(CH_2)_3Si(OH)_3 + 3CH_3OH$$

$$\text{condensation}: H_2N(CH_2)_3Si(OH)_3 + 3OH - \text{glass substrate} \rightarrow H_2N(CH_2)_3Si(O)_3 - \text{glass substrate}$$

The APS-treated IMA electrode substrate was observed by X-ray photoemission spectroscopy (XPS). The survey scan spectrum showed the presence of principal C1s, O1s, Si2p, and N1s core levels, with no evidence of impurities (Figure 1a). The N1s peak (2.1%) was observed clearly for the amino-treated substrate (Figure 1b), while there was no N1s peak for the pristine IMA substrate.

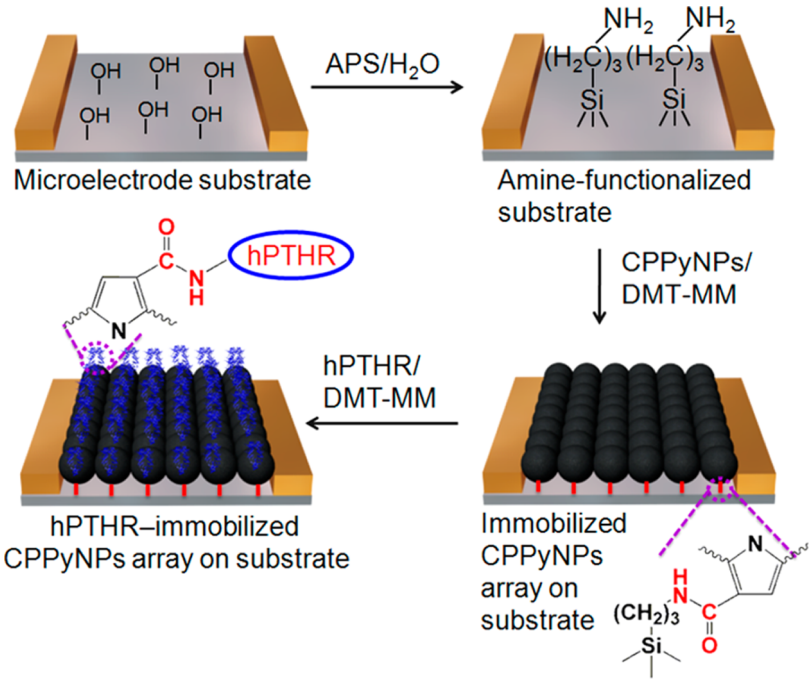

Scheme 1. Synthetic protocol of close-packed arrays of hPTHR-conjugated CPPyNPs through the immobilization process on the IMA.

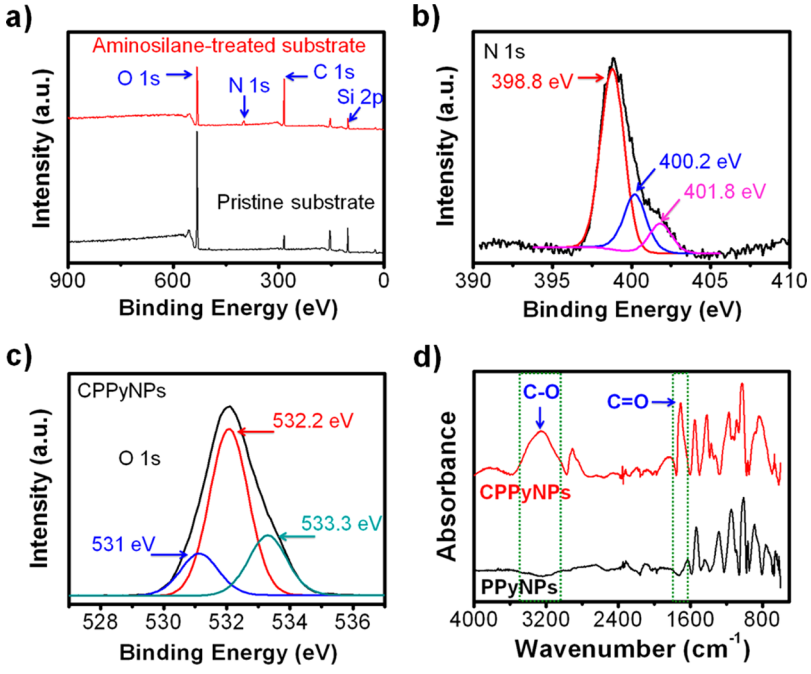

Figure 1. (a) XPS spectra of the IMA substrate before and after aminosilane treatment. (b) XPS N1s spectrum of aminosilane-treated IMA substrate. (c) XPS O1s spectrum of the CPPyNPs and (d) FT-IR spectrum of pristine PPyNPs (black line) and functionalized PPyNPs (CPPyNPs, red line).

The carboxylic groups of CPPyNPs were also identified by XPS. The survey scan spectrum showed the presence of principal C1s, O1s, and N1s core levels, with no evidence of impurities (Figure S3). The O1s peak (34.11%) was observed clearly for CPPyNPs. The O1s peak was observed clearly for PPy-NDFLG and had three components centered at 531, 532.2, and 533.3 eV, corresponding to alcohol, carbonyl, and ether-type oxygens, respectively (Figure 1c).[57] Additionally, Fourier transform infrared spectroscopy (FT-IT) was used to confirm the functionlization of the PPyNPs. The FT-IR spectra of pristine PPyNPs and CPPyNPs indicated that the carboxylic groups (−COOH) were successfully functionalized on the surface of the CPPyNPs (Figure 1d).

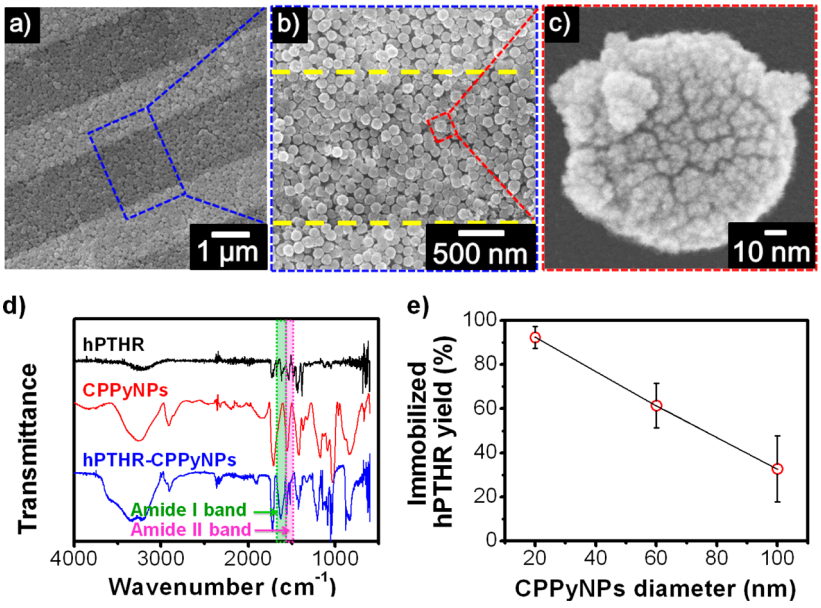

Figure 2. Typical FE-SEM images of close-packed arrays of the hPTHR-conjugated CPPyNPs on IMA substrate (the yellow dashed lines indicate boundary lines between gold electrodes). The increasing order (a < b < c) was enlarged from micrometer to nanometer length scales. (d) FT-IR spectra of hPTHR, CPPyNPs, and hPTHR-CPPyNPs. The amide I band is due to carbonyl stretching vibrations, and the amide II band is caused primarily by NH bending vibrations. (e) Calibration curve of the loading of the hPTHR on the CPPyNP surface corresponding to the diameter of the CPPyNPs.

Generally, pristine PPyNPs show a pyrrole ring stretching band at 1548 cm^{-1}, a conjugated C−N stretching band at 1473 cm^{-1}, =C−H in-plane vibration bands at 1201 and 1183 cm^{-1}, and a =C−H out-of-plane vibration band at 916 cm^{-1}. However, CPPyNPs have a distinctive broad −OH band at 3200 cm^{-1} and a sharp −C=O at 1700 cm^{-1}.[30] The modified CPPyNPs can be immobilized on the IMA electrodes and combined with various biomolecules through chemical bonding.

The fabricated CPPyNPs were immobilized on the modified IMA substrate to construct close-packed arrays. Consecutively, hPTHR was attached to the surface of the CPPyNPs. Field-emission scanning electron microscopy (FE-SEM) was used to characterize the hPTHR-conjugated CPPyNP (hPTHR-CPPyNP) nanobiohybrids[50] bound to the IMA substrate. Figure 2 displays FE-SEM images of CPPyNPs *ca.* 100 nm in diameter after the introduction of the hPTHR. The arrays of close-packed hybrid NPs were clearly observed between the IMA (Figure 2a,b) and had a rougher surface because of the attached hPTHR compared with pristine CPPyNPs (Figure 2c and Figure S4). All 20, 60, and 100 nm diameter CPPyNPs showed excellent uniformity and high densities over a scale of micrometers (Figure S4). Chemical characterization of the hPTHR-CPPyNPs was also carried out using FT-IR spectroscopy (Figure 2d). For hPTHR, the absorption peaks at 3200 cm^{-1} are attributed to stretching vibrations of alkyl, carbonyl, and amines groups. The absorption peaks in the range of 1700−1200 cm^{-1} are also ascribed to bending vibrations of amide, methyl, and methylene groups in hPTHR. The FT-IR spectrum of CPPyNPs had a broad −OH band at 3200 cm^{-1}, broad −NH band at 3300 cm^{-1}, sharp −C=O band at 1700 cm^{-1}, and strong −C−N band at 1473 and 1180−1360 cm^{-1}, while there were no significant absorption peaks corresponding to the amide I (at 1630 cm^{-1}) and II bands (at 1520 cm^{-1}) (Figure S5).[39] Interestingly, the amide I and II bands were created at the absorption peak of the hPTHR-conjugated CPPyNPs. These results indicate that hPTHR is successfully immobilized on the surface of the CPPyNPs. The loading of hPTHR on the CPPyNPs' surface was also calculated using a BCA assay (see supplementary materials of the Supporting Information). The loading of CPPyNPs increased with decreasing CPPyNP diameter (Figure 2e): 20 nm (421.04 μg hPTHR/0.5 mg CPPyNP) > 60 nm (306.09 μg hPTHR/0.5 mg CPPyNP) > 100 nm (97.18 μg hPTHR/0.5 mg CPPyNP). This is expected to lead to enhanced interaction between hPTHR and analytes. Moreover, the fluorescent dye molecules were tracked in the hPTHR using fluorescence microscopy. The immunocytochemical method was introduced with anti-GST antibody and Alexa488-conjugated anti-mouse antibody. As shown in Figure S6, the hPTHR-immobilized CPPyNPs exhibited green emission (bright region) with uniform distribution over their surfaces. There were no hPTHRs on the substrate itself, indicating that the hPTHRs were selectively attached to the oriented CPPyNP surface through direct covalent bonding.

Current−voltage (*I*−*V*) curves were measured to evaluate the electrical properties of the substrate-bound CPPyNP array. Figure 3a shows the *I*−*V* characteristics of the CPPyNP configuration before and after the introduction of hPTHR. The *I*−*V* curves were

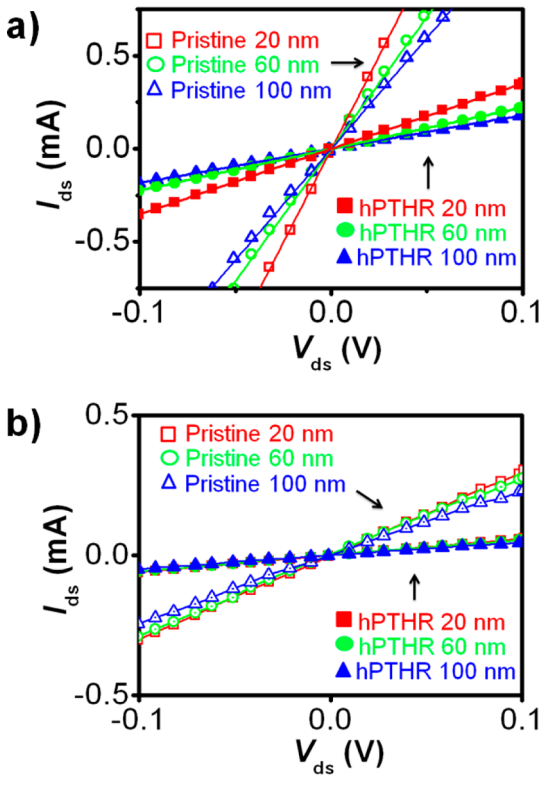

Figure 3. Comparison of current–voltage (I–V) curves of CPPyNPs 20, 60, and 100 nm bound on the IMA before and after hPTHR introduction between (a) immobilization and (b) adsorption systems (V_{ds} scan rate = 10 mV s^{-1}). (c) SEM image of hPTHR-CPPyNPs adsorbed on the IMA after the several washing processes.

linear over a voltage range from −0.1 to +0.1 V, demonstrating the ohmic behavior of the nanomaterials on the electrode substrate. The dI/dV values of the arrays increased with decreasing diameter of the CPPyNPs. Although the dI/dV value after the attachment of hPTHR decreased due to increasing resistance, the linearity of the I–V curves was maintained and the dI/dV values were consistent with those of the pristine CPPyNPs. Importantly, and in comparison with physically adsorbed systems, the electrical properties of the nanobiohybrid NPs were well-controlled by the immobilization process (Figure 3b). The dI/dV value of the 20 nm NPs chemically attached on the IMA was 10 times higher than that for adsorbed NPs. This is

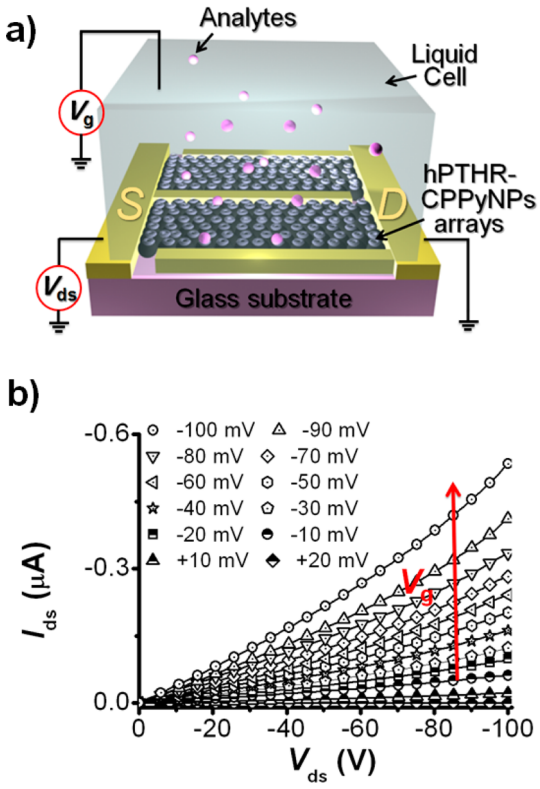

Figure 4. (a) Schematic diagram of liquid-ion-gated FET using close-packed hPTHR-CPPyNP arrays. (b) Output curves of hPTHR-conjugated CPPyNPs 20 nm FET (V_g was from +20 to −100 mV in a step of −10 mV and V_{ds} scan rate was −5 mV s^{-1}).

caused by the increase in the number of CPPyNPs detached from the IMA substrate during the repeated washing steps that are part of the process anchoring hPTHR to the surface of the CPPyNPs (Figure 3c). On the basis of these results, compact substrate-bound NP devices can maintain the reliable electrical contact and provide efficient conductive pathways for fabricating high-performance hormone sensors.

To use nanobiohybrid NPs as the signal transducing component of a biosensor, we fabricated liquid-ion-gated FETs surrounded with phosphate-buffered saline (PBS, pH 7.4) as the electrolyte. Liquid-ion gating has the advantage of making intimate contact with the nanobiohybrid NPs *via* a remote gate electrode in the surrounding electrolyte solution.[48] This strategy can be used for signal amplification to enhance the sensing performance of resistive sensors.[58] Figure 4a outlines the experimental setup used to estimate the device performance of the hPTHR-CPPyNP sensor geometry. Two interdigitated gold microelectrode bands were employed as source (*S*) and drain (*D*) electrodes. Additionally, a reference electrode was immersed in the electrolyte, and the gate potential (V_g) was applied between the reference electrode and the drain electrode through the liquid-ion solution. More than 100 devices were assessed under ambient conditions. Figure 4b demonstrates the output curves of the FET

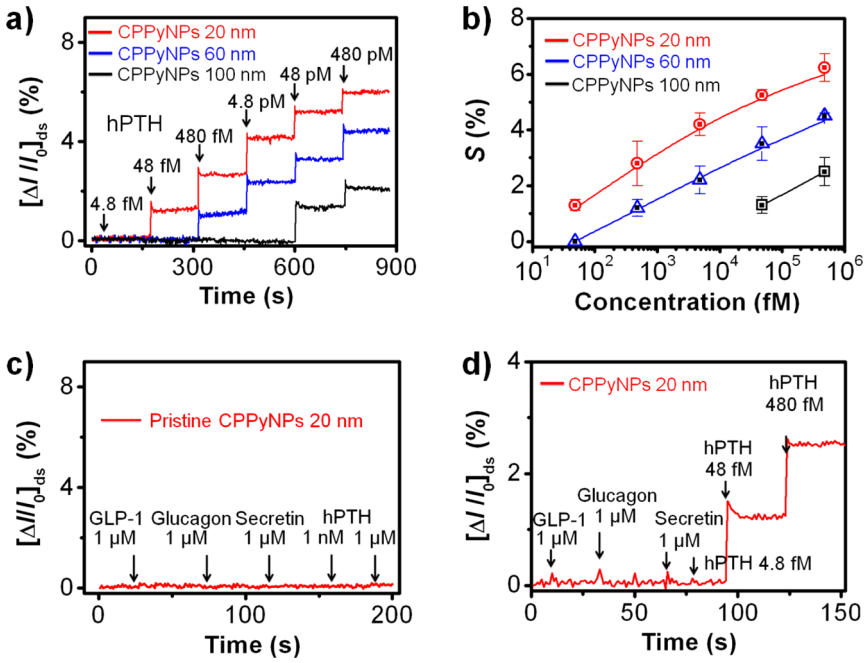

Figure 5. (a) Real-time responses with normalized current changes ($\Delta I/I_0 = (I - I_0)/I_0$, where I_0 is the initial current and I is the instantaneous current) and (b) calibration curves of hPTHR-CPPyNP hormone sensors toward various hPTH concentrations (S indicates the normalized current change). (c) Real-time responses of the pristine CPPyNP (20 nm) sensor without hPTHR measured at V_{ds} = 10 mV. Normalized I_{SD} changes upon addition of target (hPTH) and nontarget (GLP-1, glucagon, and secretin) analytes. (d) Selective responses of the hormone sensor using hPTHR-CPPyNP 20 nm toward nontarget (GLP-1, glucagon, and secretin) and target analytes.

sensor, which operated at room temperature. The drain-to-source current (I_{ds}) increased negatively with negatively increasing gate V_g, indicating p-type (hole-transporting) behavior caused by an increase in the oxidation level of the polymer chains. Accordingly, the binding of hormone biomolecules to the hPTHR-CPPyNPs immobilized between the source and drain electrodes was observed by monitoring changes in the current output through the FET devices.

To investigate the sensing characteristics of the liquid-ion-gated nanobiohybrid NP array FET, I_{ds} was monitored at V_{ds} = 10 mV (V_g = 5 mV, a low operating voltage) upon the addition of various concentrations of hPTH. The principle function of hPTHR is to bind with specific hPTHs, inducing a deformation of hPTHR. This deformation can affect the charge carrier density on the surface of the CPPyNP channels. Figure 5a displays the real-time responses of hPTHR-CPPyNP arrays using NPs with diameters of 20, 60, and 100 nm. The nanobiohybrid sensors showed a concentration-dependent increase in I_{ds} upon exposure to the target molecules (hPTHs). The current increase is likely caused by the accumulation of charge carriers (holes) elicited by the hPTH/hPTHR binding event. The specific binding of hPTH promotes a structural rearrangement in hPTHR so that the positive charges in the hPTHR can be efficiently screened. Therefore, the hPTH/hPTHR interaction induces negative point charges in the liquid-ion gate dielectric near the CPPyNPs' surface, which lead to the accumulation of positive charge carriers in the CPPyNPs channel.[47−49,54−56] This is explained by a p-type doping effect acting indirectly on the liquid-ion gate dielectric. In all measurements, the FET sensors had rapid response times of less than 1 s and showed linear responses to current changes. Signal intensities of the nanoscale FETs increased with decreasing NP diameter, consistent with the trend in increasing surface area (Figure 5b). Intriguingly, no signals toward various analytes were observed from the sensors based on the pristine CPPyNP arrays (Figure 5c), while the minimum detection level (MDL) of the FET sensor using nanobiohybrid 20 nm NPs was *ca.* 48 fM (signal-to-noise ratio = 12.5). This level of sensitivity is approximately 3−6 orders of magnitude better than that of various conventional hormone sensors.[11,59−68] Figure 5d shows the selective response of an FET sensor (20 nm CPPyNPs) toward particular hPTHs. No significant changes in I_{ds} were observed upon the addition of nontarget hormones such as GLP-1, glucagon, and secretin. These results demonstrate the excellent selectivity of the hormone sensor.

Generally, hormones coexist with various biomolecules in a living body. It is important that the biosensor is capable of detecting specific analytes. Therefore, clinically relevant samples with fetal bovine serum (FBS) were prepared to test the selectivity. Excellent selectivity was observed for FET-type hormone sensors based on nanobiohybrid 20 nm NPs arrays (Figure 6a). There were no significant signals when the bare solvent (FBS) and electrolyte (PBS) were inserted into the

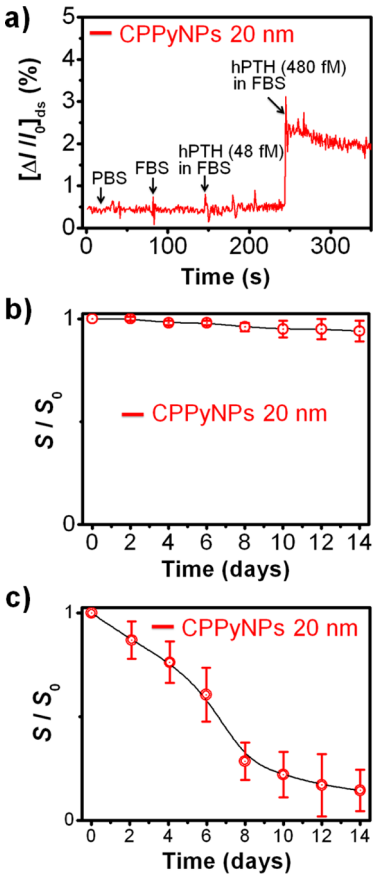

Figure 6. (a) Selective responses of nanobiohybrid NP arrays toward hPTH in FBS. Comparison with the long-term stabilities of the hormone sensor between (b) immobilization process and (c) adsorption method on the FET geometry over 2 weeks (*S* indicates normalized current changes; $S = \Delta I/I_0$).

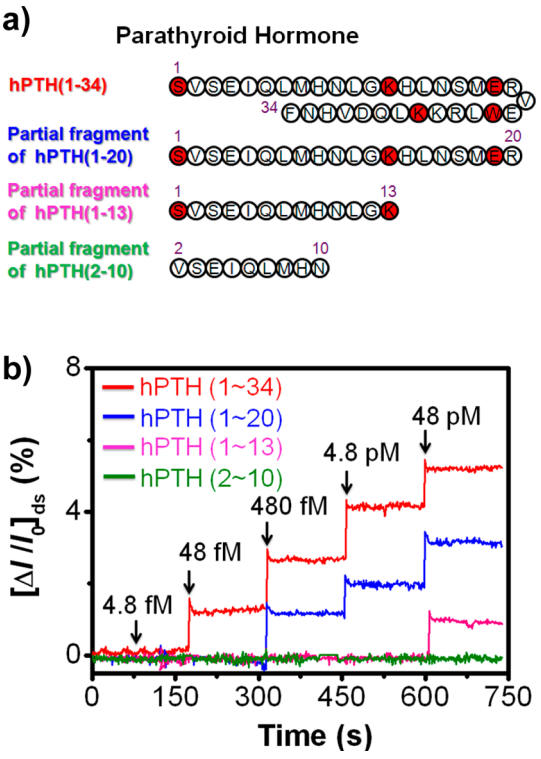

Figure 7. (a) Amino acid sequences of hPTH fragments which have a different number of critical cross-linking coordinates (red closed circles) and (b) real-time responses of the hPTHR-CPPyNP sensors upon stimulations with hPTH fragments.

hormone sensors, while the current change from hPTH was clearly confirmed (signal-to-noise = 3.6). Although, the MDL of the relevant hormone sensor was 480 fM in hPTH, this finding suggests that further optimization could provide immobilized NP arrays for practical diagnostic applications. In addition, the hormone sensor exhibited outstanding storage stability. Figure 6b shows the long-term stability of the hormone sensor toward 48 fM hPTH. The response values gradually decreased, leading to a decrease of *ca.* 8−9% in sensitivity over 2 weeks (Figure S7). Compared to the sensor systems constructed through physical adsorption, the storability of the current immobilization assay is outstanding (Figure 6c). It is evident that the lifetime of the hormone sensor in this covalent bonding system can be maintained for a long period under controlled environmental conditions.

The hPTHR/hPTH cross-linking coordinates were investigated using photoactivated amino acid side chains incorporated into hPTH analogues. To mimic the function of GPCR through the hPTHR-functionalized hormone sensor, the deleted peptide forms of hPTH having different numbers of critical cross-linking coordinates were synthesized (Figure 7a). Figure 7b displays normalized I_{ds} values that were monitored after the addition of each deletion form at various concentrations. The hPTH (1−34), an original hPTH form, had the highest sensitivity level (48 fM); the MDLs of hPTH (1−20) and hPTH (1−13) were 480 fM and 48 pM, respectively. Interestingly, the FET sensor did not respond to hPTH forms (2−10) that were excluded from the cross-linking coordinates. Therefore, peptides that have more cross-linking coordinates can elicit more sensitive responses from the nanobiohybrid sensor. These results demonstrate that CPPyNP-based FET-type hormone sensors are able to recognize each deletion form of target peptides and efficiently mimic the actual function of GPCR.

CONCLUSION

In summary, we successfully fabricated FET-type hormone sensors using an array of close-packed nanobiohybrid NPs as the signal transducer. The immobilization strategy on modified IMA substrates provided highly stable and reliable electrical properties through compact close-packed arrays of uniform, size-controlled NPs. Field-effect devices composed of nanobiohybrid NP arrays were characterized as strong p-type and were able to efficiently monitor the binding events between hPTH and hPTHR. The compact NP FETs also demonstrated the feasibility of

high-performance sensing properties at femtomolar concentrations (*ca.* 48 fM). Moreover, the hormone sensors showed long-term stability and excellent selectivity in FBS. Furthermore, the nanobiohybrid NP arrays were able to recognize deletion forms of target peptide hormones, several of the GPCR family, and identify peptide–receptor interactions using deletion mutants of peptide hormones. Therefore, the programmed FET-type hormone sensors could assist drug discovery and lead to rapid and accurate hormone analyses for disease diagnosis and management.

MATERIALS AND METHODS

Materials. Pyrrole (98%), pyrrole-3-carboxylic acid (P3CA), and $FeCl_3$ (97%) were purchased from Aldrich Chemical Co. and used without further purification. Polyvinyl alcohol (PVA) (M_w = 9000, 13 000, and 31 000) was also obtained from Aldrich.

Fabrication of Size-Controlled CPPyNPs. First, PVA was dissolved in distilled water over 5 h. The concentrations of the obtained aqueous PVA solutions were 1.25 (PVA M_w = 9000), 4.5 (PVA M_w = 13 000), and 7 (PVA M_w = 31 000) wt % relative to the amount of water. Aqueous $FeCl_3$ solution was then added. The molar ratios of aqueous $FeCl_3$ to pyrrole/P3CA were 2.5, 4.6, and 6.2 for fabricating the 20, 60, and 100 nm diameter CPPyNPs, respectively. All reactions were carried out at 28 °C. The PVA/$FeCl_3$ solutions were magnetically stirred for 3 h to equilibrate. P3CA was dissolved in pyrrole at a P3CA/pyrrole (0.5 mmol/15 mmol) molar ratio of 1/30. The pyrrole/P3CA solution (0.1 mL) was added dropwise into the PVA/$FeCl_3$ solution, and the chemical oxidation polymerization was allowed to proceed for 6 h. The resulting products were separated from dispersion solution by centrifugation (10 000 rpm, 40 min) and thoroughly washed several times with hot water to remove impurities. The remaining CPPyNP precipitates were dried in a vacuum oven at room temperature.[69]

Expression and Solubilization. hPTHR was used in this study as a model hormone receptor. It was overexpressed insolubly as GST-tag fused protein from *Escherichia coli* (*E. coli*). The hPTHR gene was amplified by PCR from a cDNA and inserted into the pENTR (Invitrogen) cloning vector using Clonase. After sequence confirmation, the hPTHR gene was transferred to pDEST15 expression vector using the GATEWAY system (Invitrogen) and checked for the presence and sequence of hPTHR by sequencing. The *E. coli* BL21 strain was transformed with pDEST15/GST-tag/hPTHR and then cultured in LB-ampicillin (50 μg mL^{-1}) medium. After induction of hPTHR with 0.5 mM IPTG, the cells were incubated at 25 °C for 4 h. Cultured cells were harvested by centrifugation at 12 000*g* for 20 min and were resuspended in PBS. The resuspended cells were lysed by sonication for 5 min, and insoluble fractions that included membrane fraction and cell debris were collected by centrifugation at 15 000*g* for 30 min. The insoluble fraction containing hPTHR was incubated with 5 vol % of Triton X-100 at room temperature during 1 h for solubilization of impurity proteins other than hPTHR, and then hPTHR was collected by centrifugation at 7000*g* for 30 min. The concentration of the collected hPTHR protein was determined by BCA assay.

Fabrication of Hormone Sensor. The liquid-ion-gated FET-type sensor platform composed of close-packed CPPyNP arrays conjugated with hormone receptors was fabricated in several stages. In the first stage, the microelectrode array interdigitated with a pair of gold electrode bands was treated with 1 wt % aqueous 3-aminopropyltrimethoxysilane (APS) solution for 6 h. A mixture of 1 wt % aqueous CPPyNPs (10 μL) and 1 wt % aqueous 4-(4,6-dimethoxy-1,3,5-triazin-2-yl)-4-methyl-morpholinium chloride (DMT-MM) solution (10 μL) was added over 12 h. The resulting CPPyNP-immobilized substrate was rinsed with distilled water. The coupling reaction was then carried out by exposing the modified substrate to a mixed solution of hPTHR and 1 wt % aqueous DMT-MM (10 μL) over 12 h to attach the hPTHR on the surface of the CPPyNPs. The substrate was then rinsed with distilled water and dried in a stream of nitrogen gas.

Instrumentation. All electrical measurements were conducted with a Keithley 2612A SourceMeter and probe station (MS TECH, Model 4000) and a Wonatech WBCS 3000 potentiostat. A chamber (300 μL volume) was designed and used for solution-based measurements. The CPPyNPs were compressed into a pellet with a thickness of 10^{-2} cm. The fluorescence microscope (Olympus, model IX2-RFA) was used for immunodetection of hPTHR on the CPPyNP surface. The excitation and emission wavelengths were 488 and 532 μm, respectively. Images were captured and processed with AnalySIS TS Auto software. A Bomem MB 100 Fourier transform infrared (FT-IR) spectrometer was used to confirm the presence of the carboxyl group (–COOH) of the CPPyNPs. Current changes were normalized as $\Delta I/I_0 = (I - I_0)/I_0$, where I_0 is the initial current and I is the instantaneous current.

Conflict of Interest: The authors declare no competing financial interest.

Acknowledgment. This work was supported by World Class University (WCU) program and Basic Science Research Program through the National Research Foundation of Korea (NRF) funded by the Ministry of Education, Science and Technology (MEST) (R31-10013), and National Research Foundation of Korea (NRF) (Grant No. 2011-0017125, 2011-0000331, 2011K000682).

Supporting Information Available: Additional information about sample preparation, characterization, and physicochemical properties, XPS, SEM, and fluorescence images. This material is available free of charge *via* the Internet at http://pubs.acs.org.

REFERENCES AND NOTES

1. Lübke, K.; Schillinger, E.; Töpert, M. Hormone Receptors. *Angew. Chem., Int. Ed. Engl.* **1976**, *15*, 741–748.
2. Schauer, R. The Mode of Action of Hormones. *Angew. Chem., Int. Ed. Engl.* **1972**, *11*, 7–16.
3. Hodsman, A. B.; Bauer, D. C.; Dempster, D. W.; Dian, L.; Hanley, D. A.; Harris, S. T.; Kendler, D. L.; McClung, D. L.; Miller, P. D.; Olszynski, W. P.; *et al.* Parathyroid Hormone and Teriparatide for the Treatment of Osteoporosis: A Review of the Evidence and Suggested Guidelines for Its Use. *Endocr. Rev.* **2005**, *26*, 688–703.
4. Hagstrom, E.; Hellman, P.; Larsson, T. E.; Ingelsson, E.; Berglund, L.; Sundstrom, J.; Melhus, H.; Held, C.; Lind, L.; Michaelsson, K.; *et al.* Plasma Parathyroid Hormone and the Risk of Cardiovascular Mortality in the Community. *Circulation* **2009**, *119*, 2765–2771.
5. Mannstadt, M.; Juppner, H.; Gardella, T. J. Receptors for PTH and PTHrP: Their Biological Importance and Functional Properties. *Am. J. Physiol.* **1999**, *277*, F665–F675.
6. Downs, T. M.; Burton, D. W.; Araiza, F. L.; Hastings, R. H.; Deftos, L. J. PTHrP Stimulates Prostate Cancer Cell Growth and Upregulates Aldo-Keto Reductase 1C3. *Cancer Lett.* **2011**, *306*, 52–59.
7. Bompart, M.; Wilde, Y. D.; Haupt, K. Chemical Nanosensors Based on Composite Molecularly Imprinted Polymer Particles and Surface-Enhanced Raman Scattering. *Adv. Mater.* **2010**, *22*, 2343–2348.
8. Lequin, R. M. Enzyme Immunoassay (EIA)/Enzyme-Linked Immunosorbent Assay (ELISA). *Clin. Chem.* **2005**, *51*, 2415–2418.

9. Opitz, N.; Lubbers, D. Electrochromic Dyes, Enzyme Reactions and Hormone−Protein Interactions in Fluorescence Optic Sensor (Optode) Technology. *Talanta* **1988**, *35*, 123–127.
10. Pritchard, D.; Morgan, H.; Cooper, J. Simultaneous Determination of Follicle Stimulating Hormone and Luteinising Hormone Using a Multianalyte Immunosensor. *Anal. Chim. Acta* **1995**, *310*, 251–256.
11. Matsuura, H.; Sato, Y.; Niwa, O.; Mizutani, F. Electrochemical Enzyme Immunoassay of a Peptide Hormone at Picomolar Levels. *Anal. Chem.* **2005**, *77*, 4235–4240.
12. Harding, P. J.; Hadingham, T. C.; McDonnell, J. M.; Watts, A. Direct Analysis of a GPCR-Agonist Interaction by Surface Plasmon Resonance. *Eur. Biophys. J.* **2006**, *35*, 709–712.
13. Ruach-Nir, I.; Bendikov, T. A.; Doron-Mor, I.; Barkay, Z.; Vaskevich, A.; Rubinstein, I. Silica-Stabilized Gold Island Films for Transmission Localized Surface Plasmon Sensing. *J. Am. Chem. Soc.* **2007**, *129*, 84–92.
14. Merkoci, A. Nanoparticles-Based Stratagies for DNA, Protein and Cell Sensors. *Biosen. Bioelectron.* **2010**, *26*, 1164–1177.
15. Soreni-Harari, M.; Mocatta, D.; Zimin, M.; Gannot, Y.; Banin, U.; Tessler, N. Interface Modifications of InAs Quantum-Dots Solids and Their Effects on FET Performance. *Adv. Funct. Mater.* **2010**, *20*, 1005–1010.
16. Star, A.; Gabriel, J.-C.; Bradley, K.; Gruner, G. Electronic Detection of Specific Protein Binding Using Nanotube FET Devices. *Nano Lett.* **2003**, *3*, 459–463.
17. Zheng, H.; Lee, I.; Rubner, M. F.; Hammond, P. T. Two Component Particle Arrays on Patterned Polyelectrolyte Multilayer Templates. *Adv. Mater.* **2002**, *14*, 569–572.
18. Campbell, F. W.; Belding, S. R.; Baron, R.; Xiao, L.; Compton, R. G. Hydrogen Peroxide Electroreduction at a Silver-Nanoparticle Array: Investigating Nanoparticle Size and Coverage Effects. *J. Phys. Chem. C* **2009**, *113*, 9053–9062.
19. Wen, T.; Majetich, S. A. Ultra-Large-Area Self-Assembled Monolayers of Nanoparticles. *ACS Nano* **2011**, *5*, 8868–8876.
20. Vijayalakshmi, A.; Tarunashree, Y.; Baruwati, B.; Manorama, S. V.; Narayana, B. L.; Johnson, R. E. C.; Rao, N. M. Enzyme Field Effect Transistor (ENFET) for Estimation of Triglycerides Using Magnetic Nanoparticles. *Biosens. Bioelectron.* **2008**, *23*, 1708–1714.
21. Makowski, M. S.; Ivanisevic, A. Molecular Analysis of Blood with Micro-/Nanoscale Field-Effect-Transistor Biosensors. *Small* **2011**, *7*, 1863–1875.
22. Lee, J.-S.; Han, M. S.; Mirkin, C. A. Colorimetric Detection of Mercuric Ion (Hg2+) in Aqueous Media Using DNA-Functionalized Gold Nanoparticles. *Angew. Chem., Int. Ed.* **2007**, *46*, 4093–4096.
23. Song, Y.; Wei, W.; Qu, X. Colorimetric Biosensing Using Smart Materials. *Adv. Mater.* **2011**, *23*, 4215–4236.
24. Katz, E.; Willner, I. Integrated Nanoparticle−Biomolecule Hybrid Systems: Synthesis, Properties, and Applications. *Angew. Chem., Int. Ed.* **2004**, *43*, 6042–6108.
25. Goesmann, H.; Feldmann, C. Nanoparticulate Functional Materials. *Angew. Chem., Int. Ed.* **2010**, *49*, 1362–1395.
26. Riha, S. C.; Johnson, D. C.; Prieto, A. L. Cu_2Se Nanoparticles with Tunable Electronic Properties Due to a Controlled Solid-State Phase Transition Driven by Copper Oxidation and Cationic Conduction. *J. Am. Chem. Soc.* **2010**, *133*, 1383–1390.
27. Winter, A.; Hager, M. D.; Newkome, G. R.; Schubert, U. S. The Marriage of Terpyridines and Inorganic Nanoparticles: Synthetic Aspects, Characterization Techniques, and Potential Applications. *Adv. Mater.* **2011**, *23*, 5728–5748.
28. Yu, X.; Rotello, V. M. Nanoparticle Devices: Going with the Electron Flow. *Nat. Nanotechnol.* **2011**, *6*, 693–694.
29. Gao, Y.; Tang, Z. Design and Application of Inorganic Nanoparticle Superstructures: Current Status and Future Challenges. *Small* **2011**, *7*, 2133–2146.
30. Vaddiraju, S.; Seneca, K.; Gleason, K. K. Novel Strategies for the Deposition of COOH Functionalized Conducting Copolymer Films and the Assembly of Inorganic Nanoparticles on Conducting Polymer Platforms. *Adv. Funct. Mater.* **2008**, *18*, 1929–1938.
31. Yathindranath, V.; Rebbouh, L.; Moore, D. F.; Miller, D. W.; Lierop, J.; Hegmann, T. A Versatile Method for the Reductive, One-Pot Synthesis of Bare, Hydrophilic and Hydrophobic Magnetite Nanoparticles. *Adv. Funct. Mater.* **2011**, *21*, 1457–1464.
32. Bae, A.-H.; Numata, M.; Hasegawa, T.; Li, C.; Kaneko, K.; Sakurai, K.; Shinkai, S. 1D Arrangement of Au Nanoparticles by the Helical Structure of Schizophyllan: A Unique Encounter of a Natural Product with Inorganic Compounds. *Angew. Chem., Int. Ed.* **2005**, *44*, 2030–2033.
33. Bunz, U. H. F.; Rotello, V. M. Gold Nanoparticle−Fluorophore Complexes: Sensitive and Discerning "Noses" for Biosystems Sensing. *Angew. Chem., Int. Ed.* **2010**, *49*, 3268–3279.
34. Srinivasan, B.; Li, Y.; Jing, Y.; Xu, Y.; Yao, X.; Xing, C.; Wang, J.-P. A Detection System Based on Giant Magnetoresistive Sensors and High-Moment Magnetic Nanoparticles Demonstrates Zeptomole Sensitivity: Potential for Personalized Medicine. *Angew. Chem., Int. Ed.* **2009**, *48*, 2764–2767.
35. Tin, Y.; Xia, Y. Self-Assembly of Spherical Colloids into Helical Chains with Well-Controlled Handedness. *J. Am. Chem. Soc.* **2003**, *125*, 2048–2049.
36. Jang, J.; Oh, J. H.; Stucky, G. D. Fabrication of Ultrafine Conducting Polymer and Graphite Nanoparticles. *Angew. Chem., Int. Ed.* **2002**, *41*, 4016–4019.
37. Jang, J. Conducting Polymer Nanomaterials and Their Applications. *Adv. Polym. Sci.* **2006**, *199*, 189–259.
38. Yoon, H.; Choi, M; Lee, K. J.; Jang, J. Versatile Strategies for Fabricating Polymer Nanomaterials with Controlled Size and Morphology. *Macromol. Res.* **2008**, *16*, 85–102.
39. Yoon, H.; Jang, J. Conducting-Polymer Nanomaterials for High-Performance Sensor Applications: Issues and Challenges. *Adv. Funct. Mater.* **2009**, *19*, 1567–1576.
40. Potyrailo, R. A. Polymeric Sensor Materials: Toward an Alliance of Combinatorial and Rational Design Tools? *Angew. Chem., Int. Ed.* **2006**, *45*, 702–723.
41. Hassan, A. Q.; Koh, J. T. Selective Chemical Rescue of a Thyroid-Hormone-Receptor Mutant, TRβ(H435Y), Identified in Pituitary Carcinoma and Resistance to Thyroid Hormone. *Angew. Chem., Int. Ed.* **2008**, *47*, 7280–7283.
42. Segre, S. V.; Goldring, S. R. Receptors for Secretin, Calcitonin, Parathyroid Hormone (PTH)/PTH-Related Peptide, Vasoactive Intestinal Peptide, Glucagonlike Peptide 1, Growth Hormone-Releasing Hormone, and Glucagon Belong to a Newly Discovered G-Protein-Linked Receptor Family. *Trends Endocrinol. Metab.* **1993**, *4*, 309–314.
43. Michalke, K.; Huyghe, C.; Lichière, J.; Gravière, M. E.; Siponen, M.; Sciara, G.; Lepaul, I.; Wagner, R.; Magg, C.; Rudolph, R. Mammalian G Protein-Coupled Receptor Expression in *Escherichia coli*: II. Refolding and Biophysical Characterization of Mouse Cannabinoid Receptor 1 and Human Parathyroid Hormone Receptor 1. *Anal. Biochem.* **2010**, *401*, 74–80.
44. Beck-Sickinger, A. G.; Budisa, N. Genetically Encoded Photocrosslinkers as Molecular Probes to Study G-Protein-Coupled Receptors (GPCRs). *Angew. Chem., Int. Ed.* **2012**, *51*, 310–312.
45. Gliman, A. G. G Proteins and Regulation of Adenylate Cyclase (Nobel Lecture). *Angew. Chem., Int. Ed.* **1995**, *34*, 1406–1419.
46. Sarramegn, V.; Muller, I.; Milon, A.; Talmont, F. Recombinant G Protein-Coupled Receptors from Expression to Renaturation: A Challenge towards Structure. *Cell. Mol. Life Sci.* **2006**, *63*, 1149–1164.
47. Kwon, O. S.; Park, S. J.; Jang, J. A High-Performance VEGF Aptamer Functionalized Polypyrrole Nanotube Biosensor. *Biomaterials* **2010**, *31*, 4740–4747.
48. Yoon, H.; Lee, S. H.; Kwon, O. S.; Park, T. H.; Jang, J. Polypyrrole Nanotubes Conjugated with Human Olfactory Receptors: High-Performance Transducers for FET-Type Bioelectronic Noses. *Angew. Chem., Int. Ed.* **2009**, *48*, 2755–2758.

49. Kwon, O. S.; Hong, T. J.; Kim, S. K.; Jeong, J. H.; Hahn, J. S.; Jang, J. Hsp90-Functionalized Polypyrrole Nanotube FET Sensor for Anti-cancer Agent Detection. *Biosens. Bioelectron.* **2010**, *25*, 1307–1312.
50. Willner, I.; Willner, B. Biomolecule-Based Nanomaterials and Nanostructures. *Nano Lett.* **2010**, *10*, 3805–3815.
51. De, M.; Ghosh, P. S.; Rotello, V. M. Applications of Nanoparticles in Biology. *Adv. Mater.* **2008**, *20*, 4225–4241.
52. Engel, Y.; Elnathan, R.; Pevzner, A.; Davidi, G.; Flaxer, E.; Patolsky, F. Supersensitive Detection of Explosives by Silicon Nanowire Arrays. *Angew. Chem., Int. Ed.* **2010**, *49*, 6830–6835.
53. Kwon, O. S.; Hong, J. Y.; Park, S. J.; Jang, Y.; Jang, J. Resistive Gas Sensors Based on Precisely Size-Controlled Polypyrrole Nanoparticles: Effects of Particle Size and Deposition Method. *J. Phys. Chem. C* **2010**, *114*, 18874–18879.
54. Song, H. S.; Lee, S. H.; Oh, E. H.; Park, T. H. Expression, Solubilization and Purification of a Human Olfactory Receptor from *Escherichia coli*. *Curr. Microbiol.* **2009**, *59*, 309–314.
55. Kim, T. H.; Lee, S. H.; Lee, J.; Song, H. S.; Oh, E. H.; Park, T. H.; Hong, S. Single-Carbon-Atomic-Resolution Detection of Odorant Molecules Using a Human Olfactory Receptor-Based Bioelectronic Nose. *Adv. Mater.* **2009**, *21*, 91–94.
56. Kim, T. H.; Song, H. S.; Jin, H. J.; Lee, S. H.; Namgung, S.; Kim, U.; Park, T. H.; Hong, S. "Bioelectronic Super-Taster" Device Based on Taste Receptor−Carbon Nanotube Hybrid Structures. *Lab Chip* **2011**, *11*, 2262–2267.
57. López, G. P.; Castner, D. G.; Ratner, B. D. XPS O 1s Binding Energies for Polymers Containing Hydroxyl, Ether, Ketone and Ester Groups. *Surf. Interface Anal.* **1991**, *17*, 267–272.
58. Alam, M. M.; Wang, J.; Guo, Y.; Lee, S. P.; Tseng, H. R. Electrolyte-Gated Transistors Based on Conducting Polymer Nanowire Junction Arrays. *J. Phys. Chem. B* **2005**, *109*, 12777–12784.
59. Pritchard, D. J.; Morgan, H.; Cooper, J. M. Simultaneous Determination of Follicle Stimulating Hormone and Luteinising Hormone Using a Multianalyte Immunosensor. *Anal. Chim. Acta* **1995**, *310*, 251–256.
60. Wang, F.; Yang, J.; Wu, K. Mesoporous Silica-Based Electrochemical Sensor for Sensitive Determination of Environmental Hormone Bisphenol A. *Anal. Chim. Acta* **2009**, *638*, 23–28.
61. Hage, D. S.; Kao, P. C. High-Performance Immunoaffinity Chromatography and Chemiluminescent Detection in the Automation of a Parathyroid Hormone Sandwich Immunoassay. *Anal. Chem.* **1991**, *63*, 586–595.
62. Sesay, A. M.; Cullen, D. C. Detection of Hormone Mimics in Water Using a Miniaturised SPR Sensor. *Environ. Monit. Assess.* **2001**, *70*, 83–92.
63. Fuchs, S.; Haimovich, J.; Fuchs, Y. Immunological Studies of Plant Hormones. *Eur. J. Biochem.* **1971**, *18*, 384–390.
64. Gan, T.; Hu, C.; Chen, Z.; Hu, S. Fabrication and Application of a Novel Plant Hormone Sensor for the Determination of Methyl Jasmonate Based on Self-Assembling of Phosphotungstic Acid−Graphene Oxide Nanohybrid on Graphite Electrode. *Sens. Actuators, B* **2010**, *151*, 8–14.
65. Bangar, M. A.; Shirale, D. J.; Chen, W.; Myung, N. V.; Mulchandani, A. Single Conducting Polymer Nanowire Chemiresistive Label-Free Immunosensor for Cancer Biomarker. *Anal. Chem.* **2009**, *81*, 2168–2175.
66. Barceló, B.; Ayllón, O.; Belmonte, M.; Barceló, A.; Vidal, R.; Forteza-Rey, J.; Gutiérrez, A. Proposed Reference Value of the CA 125 Tumour Marker in Men. Potential Applications in Clinical Practice. *Clin. Biochem.* **2008**, *41*, 717–722.
67. Hernandex, J.; Thompson, I. M. Prostate-Specific Antigen: A Review of the Validation of the Most Commonly Used Cancer Biomarker. *Cancer* **2004**, *101*, 894–904.
68. Treviño, J.; Calle, A.; Rodríguez-Frade, J. M.; Mellado, M.; Lechuga, L. M. Surface Plasmon Resonance Immunoassay Analysis of Pituitary Hormones in Urine and Serum Samples. *Clin. Chim. Acta* **2009**, *403*, 56–62.
69. Hong, J. Y.; Yoon, H.; Jang, J. Kinetic Study of the Formation of Polypyrrole Nanoparticles in Water-Soluble Polymer/Metal Cation Systems: A Light-Scattering Analysis. *Small* **2010**, *6*, 679–686.